

# ON THE COHERENCE PROPERTIES OF DIFFERENT FEL

- A simulation approach -

A Thesis submitted for the degree of Master in Synchrotron Radiation Based Science  
by

**Mihai Pop**

Lund University, Faculty of Science, MAX Faculty of Science

Master thesis supervised by  
Francesca Curbis and Sverker Werin



**LUND**  
UNIVERSITY





## **Abstract**

Free Electron Lasers (FEL) are one of the most brilliant light sources in the world and due to their unique properties they are used to push the frontier of knowledge in fields such as biochemistry and protein crystallography. This is the reason why there is a lot of research worldwide about understanding and improving them. Although there are numerous papers describing the output of the FEL in terms of coherence and bandwidth, it is not clear how this coherence evolves or what the factors that influence it the most are. For this reason I propose analyzing the radiation as it is being produced, inside the undulator, with the aid of simulations. The tools developed for this analysis make use of programming and data processing software to recreate well known experiments used in coherence studies. These virtual tools can serve as good initial approximations for changing different parameters or designing new types of FEL, as well as improving the fundamental knowledge of the FEL process. This work uses the developed tools to characterize a particular FEL layout and extract meaningful information with respect to its coherence properties.



# Contents

<b>1</b>	<b>Introduction</b>	<b>2</b>
<b>2</b>	<b>The Free electron Laser</b>	<b>3</b>
2.1	Undulator radiation . . . . .	3
2.1.1	Undulator radiation wavelength . . . . .	4
2.1.2	Undulator radiation bandwidth . . . . .	4
2.2	FEL Radiation . . . . .	5
2.2.1	Microbunching . . . . .	5
2.2.2	Statistical properties of FEL . . . . .	6
2.2.3	SASE and Seeded FEL . . . . .	8
<b>3</b>	<b>Coherence</b>	<b>10</b>
3.1	Longitudinal coherence and Spectral density . . . . .	10
3.2	Transverse coherence and Young's experiment . . . . .	12
<b>4</b>	<b>Simulations</b>	<b>14</b>
4.1	Overview of <i>Genesis 1.3</i> . . . . .	14
4.1.1	Input and output . . . . .	16
4.2	Analysis . . . . .	17
4.2.1	Spectrum and coherence time . . . . .	17
4.3	Virtual Young's experiment . . . . .	18
<b>5</b>	<b>Results and discussions</b>	<b>21</b>
5.1	Longitudinal coherence results . . . . .	22
5.2	Transverse coherence results . . . . .	25
<b>6</b>	<b>Conclusions and outlook</b>	<b>31</b>
<b>7</b>	<b>Appendices</b>	<b>34</b>



## Conventions and list of commonly used symbols

- *LINAC* - Linear accelerator
- $\beta = \frac{v}{c}$  - ratio between an electron's velocity and the speed of light
- $\gamma = \frac{E_{tot}}{E_{rest}} = \frac{1}{\sqrt{1-\beta^2}}$  - Lorentz factor for electron
- *e.m.* - electromagnetic
- *FEL* - Free Electron Laser
- *SASE* - Self Amplified Spontaneous Emission
- *TD* - Time dependent
- *TI* - Time independent
- *FT* - Fourier Transform
- $R_L$  - Rayleigh length
- *FWHM* - Full width at half maximum





# 1 Introduction

Free electron Lasers use the kinetic energy of relativistic electrons and transform it into electromagnetic radiation with the use of a periodic magnetic structure called undulator. While traveling through the undulator electrons emit coherent radiation due to their interaction with the electric field of the radiation.

In this project the aim was to develop virtual tools to study how coherence builds up in an FEL and to investigate how changing different parameters affects these coherence properties. Numerical simulations have been widely used in literature [1, 2, 3] due to their cost effectiveness and flexibility in changing any construction parameter of the FEL. To extract coherence information from the simulations, we devised virtual experiments that follow the physics of real experiments. The method was tested on a specific FEL layout and coherence information was extracted by following some key steps :

- Simulate an FEL using the *Genesis 1.3* software,
- Read the output radiation files in a comprehensive way
- Devise ways to extract information about the radiation coherence properties
- Follow how changing parameters of the FEL changes these properties.

The motivation for this project is the fact that in the theoretical description of the FEL process, a lot of variables come into play and the sheer number of parameters makes the mathematics involved become lengthy. Therefore I developed a method that analyzes the radiation by mimicking simple experimental techniques. In [4, 5, 6] the transverse coherence properties are studied using the Young experiment, while the longitudinal coherence is studied in [7, 8] with Fourier analysis. That is why, the methods used here for coherence studies are the Young experiment for transverse properties and the Fourier or spectral analysis for longitudinal coherence. Although in experimental work [9] the Michaelson Interferometers is used, for numerical simulations the Fourier analysis is preferred [10].

Even though the results presented here are not quantitative, they highlight the existing physics and can become useful when comparing different parameter changes that one might consider in an FEL. Furthermore, since the analysis tools are based on an existing experimental concept, it would be possible to implement an experiment and compare the results from simulations with actual experimental results. The results concerning the light at different positions in the undulator might be coupled with the electron distribution and bunching information to better understand the exponential gain and saturation processes.

This report is divided into four main sections, the first of which is a presentation of the physics behind the FEL, readers with experience in this field can skip this part. The second section will go through the basic concepts of coherence that I use in my studies. The techniques used in these simulations and the code created to extract the coherence properties will be described in the third section. The final part will be reserved to presenting actual coherence results of an FEL layout example and comparing these results when some FEL parameters are changed.

## 2 The Free electron Laser

*This section is meant as an introduction to the physics behind the FEL and as a walk through of the most important FEL properties.*

The basic layout of an FEL is shown in Figure 1. The electron gun produces bunches of electrons that are accelerated in a linear accelerator (LINAC) to relativistic energies. After the acceleration, bunches of electrons enter the undulator where they emit electromagnetic radiation. Along the undulator, the electron bunch interacts with the radiation produced at the beginning of the undulator and through this interaction microbunches are formed. The separation of these microbunches exactly matches the radiation wavelength therefore the radiation emitted by the electrons is phase matched.

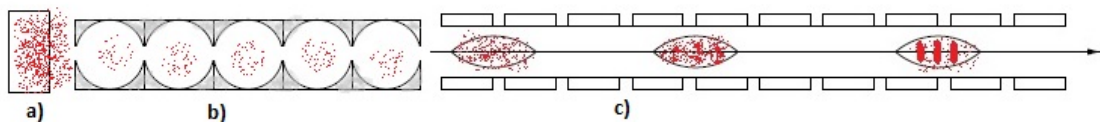


**Figure 1:** Schematic representation of the FEL layout. a) The electron gun b) the Linear accelerator (LINAC) c) The undulator section.

### 2.1 Undulator radiation

Since the FEL is basically a long undulator, it is worthwhile to look at how undulator radiation is produced and what its properties are. The driving mechanism of undulator radiation is based on electrodynamic effects of electrons at relativistic velocities passing through a periodic magnetic field perpendicular to their motion.

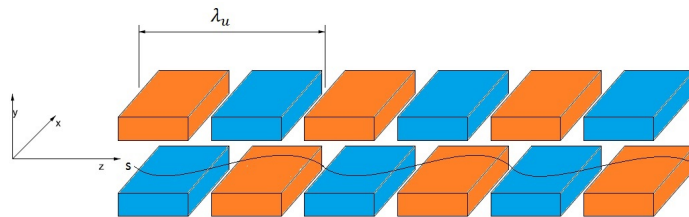


**Figure 2:** Schematic representation of the periodic magnetic arrangement in an undulator

In Figure 2 the distance between two points with the same magnetic field is called the period of the undulator and is denoted by  $\lambda_u$ . The variation in intensity of the magnetic field is consistent with a sine function  $\vec{B} = B_0 \sin(k_u z) \vec{e}_y$ , [11] where  $k_u = \frac{2\pi}{\lambda_u}$ . Given this dependence of the magnetic field with respect to  $z$  (which in our case is the propagation direction of the electron bunch entering the undulator) one electron's path follows the sinusoidal line "S" in Figure 2. When describing the electron motion we use the coordinate system depicted in Figure 2. The side motion is in the  $x$  direction and it can be written in the first order approximation as [11]:

$$x(z) = \frac{K}{k_u \beta \gamma} \sin(k_u z). \quad (2.1)$$

In equation 2.1,  $K$  is the unitless undulator parameter, with its analytical form:  $K = \frac{eB_0 \lambda_u}{2\pi m_e c} = 0.934 B_0 [T] \lambda_u [cm]$  [12], . The first order approximation assumes that the velocity in the  $z$  direction is constant and that it is much larger than that in  $x$  direction  $\dot{z} \gg \dot{x}$ ,  $\dot{z} = const$ .

The perturbation introduced to the velocity along  $z$  by the magnetic field of the undulator is:  $v_z(t) = c[1 - \frac{1}{2\gamma^2}(\frac{\beta^2 K^2}{2}(1 - \cos(2\omega_u t)))]$ , which consists of an average velocity

$$v_z(t) = c[1 - \frac{\beta^2 K^2}{4\gamma^2}] = \bar{\beta}c. \quad (2.2)$$

and an oscillating term:

$$v_z(t) = c[\frac{\beta^2 K^2}{4\gamma^2} \cos(2\omega_u t).] \quad (2.3)$$

### 2.1.1 Undulator radiation wavelength

In the laboratory frame of reference the electron oscillates in the  $x$  direction with  $\omega_u = \frac{2\pi c}{\lambda_u}$ . To correctly calculate the wavelength of the radiation, we first move into the frame of reference traveling at the average velocity from equation 2.2. In the Lorentz transformation we use the modified gamma parameter,  $\bar{\gamma} = \frac{1}{\sqrt{1-\bar{\beta}^2}}$ , since our frame of reference is moving with  $\bar{\beta}$  average relative velocity. We find that in this frame of reference the electron "sees" the magnetic structure as having a period of  $\lambda_u^* = \frac{\lambda_u}{\bar{\gamma}}$  and has an angular velocity of  $\omega_u^* = \bar{\gamma}\omega_u$ .

Due to this oscillation, the electron emits dipole radiation with the same frequency  $\omega_u^*$  and the corresponding photon energy  $\hbar\omega^*$ . In order to observe that radiation, we must revert to the laboratory frame of reference using the relativistic Doppler effect. The photon frequency in the laboratory frame of reference is [11]  $\omega_{lab} = \frac{\omega^*}{\bar{\gamma}(1-\bar{\beta}\cos\theta)}$  with the corresponding wavelength  $\lambda_{lab} = \frac{2\pi c}{\omega_{lab}} = \frac{2\pi c}{\bar{\gamma}\omega_u} \bar{\gamma}(1-\bar{\beta}\cos\theta) = \lambda_u(1-\bar{\beta}\cos\theta)$ . Using the approximations for small angles,  $\cos\theta = 1 - \frac{\theta^2}{2}$  and the definition of  $\bar{\beta}$  from equation 2.2, we arrive at the well known formula for undulator radiation wavelength:

$$\lambda_{lab} = \frac{\lambda_u}{2\gamma^2} (1 + \frac{K^2}{2} + \gamma^2 \theta^2) \quad (2.4)$$

### 2.1.2 Undulator radiation bandwidth

We consider an electron passing through  $N$  undulator periods in a time duration  $T = N * \lambda/c$ , we can write the electric field as  $E = E_0 \exp(-i\omega_{lab}t)$  where  $\omega_{lab}$  is the radiation frequency in the laboratory frame of reference. To obtain the frequency spectrum we use the Fourier transform keeping in mind that the beam is finite in time  $F(\omega) = \int_{-T/2}^{T/2} E(t) * \exp(i\omega t) dt = E_0 \int_{-T/2}^{T/2} \exp(-i(\omega_{lab} - \omega)t) dt = 2E_0 \frac{\sin((\omega_{lab} - \omega)T/2)}{\omega_{lab} - \omega}$ . The spectral intensity is  $I(\omega) = |F(\omega)|^2$  which is proportional to  $(\sin(x)/x)^2$  with  $x = (\omega_{lab} - \omega)T/2$ . This is a *sinc* function that has the maximum at  $x = 0$  and the FWHM at  $x = \pi$ , which means the bandwidth of the radiation is:  $\Delta\omega = \omega_{lab} - \omega = \frac{\omega_{lab}}{N}$ .

## 2.2 FEL Radiation

In this subsection we will describe the processes happening in an FEL without going into the lengthy mathematics. However we will present some key FEL parameters that will be of use latter on.

We first address the fundamentals of the interaction between light and the electron bunch. In this analysis we consider an electromagnetic wave traveling with the electron beam. Within the span of one wavelength of the e.m. field, the electric field is distributed along the  $z$  axis as depicted in Figure 3. This means that the electric field of the radiation will act on the electrons in a direction that is perpendicular to the  $z$  axis.

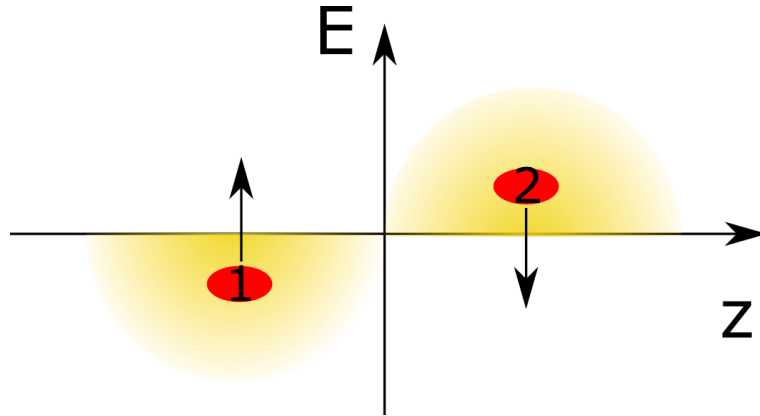


**Figure 3:** Schematic representation of the forces acting on electrons in an electromagnetic wave

### 2.2.1 Microbunching

As previously discussed, the electrons have a wiggling motion due to the magnetic field of the undulator aside from the main velocity component. Depending on the position in the undulator period and on the position relative to the radiation wavelength, the electrons can either gain or lose energy from the field. In Figure 4, an illustrative example of this effect is shown. In its wiggling motion, electron "1" gains energy from the e.m. field because the force acting on it from the electric field is in the same direction as its transverse motion. The reverse is true for electron "2".

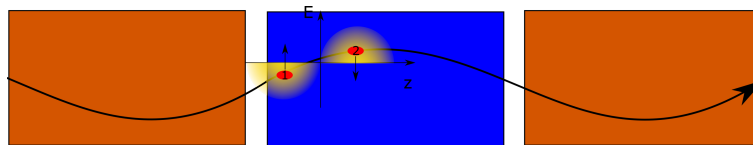


**Figure 4:** Schematic representation of the interaction of two electrons in an undulator with the electromagnetic field in a half of undulator period. Electron "1" gains energy while electron "2" loses energy

The wavelength of the radiation and the electron size are greatly exaggerated for visualization purposes but one can imagine how the electrons become modulated in energy. Periodically along the  $z$  axis, with a period of  $\lambda_{lab}$ , there are electrons that lose or gain energy through this interaction. This energy transfer between electrons and light has to be done in a steady state to have a noticeable effect. The condition for having a steady energy exchange is that the light "slips" ahead by an integer number of  $\frac{\lambda_{lab}}{2}$  in an undulator half period. This condition is called **slippage** and holds an important role in designing any FEL.

Light travels faster than the electrons mainly because of their wiggling trajectory. The average velocity of the electrons in the  $z$  direction is given by equation 2.2. Through simple algebra we arrive at the following condition for slippage:

$$\lambda_{lab} = \frac{\lambda_u}{2\gamma^2} \left(1 + \frac{K^2}{2}\right) \quad (2.5)$$

Let us now examine what happens to electrons of different energies traveling through the undulator. At relativistic velocities a slight energy change has little effect on the speed of the electron. More energetic electrons have trajectories less bent by the magnetic field than the trajectories of less energetic ones [13].

Continuing with the above argument we can reason that more energetic electrons are bent less in the undulator thus having a shorter path. Because the electrons have approximately the same velocity, the more energetic ones will skip ahead while the less energetic ones will lag behind. This effect transforms the energy modulation from the interaction with the electromagnetic field, into spatial modulation along the  $z$  axis.

We define  $\phi$  as the relative phase between a particle and the electromagnetic phase. For example in Figure 3, the first particle has negative relative phase and the second one has positive relative phase. We can see that particles with negative phase take energy from the field while particles with positive phase give energy to the field. There are also particles with nominal energy and zero phase, that do not exchange energy with the field.

An electron bunch is far larger than the radiation wavelength, so within a big bunch, smaller bunches start to form due to the interactions described above. Within each period of the e.m. wave, electrons lose or gain energy and start to bunch up. These new smaller bunches are called microbunches and have the property that the light emitted from them has the same phase. This phase correlation means that the intensity is proportional to the square of the number of electrons that have this modulation [12].

### 2.2.2 Statistical properties of FEL

So far we have not cared where the radiation that interacts with the electrons comes from, in fact, the radiation is being produced by the electrons themselves. As the light produced in the early stages of the undulator starts to make its way through the electron beam, due to slippage, it bunches up the electrons. These newly modulated electrons emit radiation that is in phase with the radiation that generated the bunching. Having more intensity at a

specific wavelength and phase increases the bunching effect, which in turn increases the light intensity. This is a process that grows exponentially. As can be seen in Figure 5, the process reaches a saturation when no more bunching can be achieved.

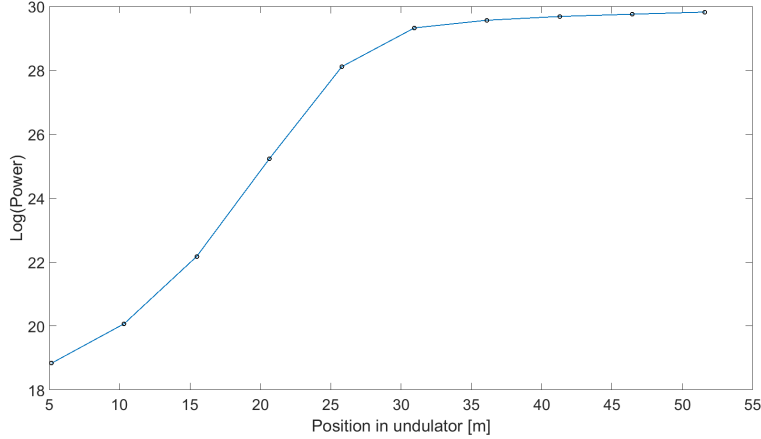


**Figure 5:** Logarithmic plot of the power versus position in the undulator, showing the exponential behavior of the output power. Data obtained from *Genesis 1.3* simulation

The mathematics in deriving the e.m. field produced by the electrons as they pass through the undulator is lengthy and beyond the scope of this work, for more information on this matter please refer to [11]. We will however highlight several key parameters that come out of this derivation. The FEL acts like an amplifier for the e.m. field. Many parameters of interest such as the bandwidth and gain, are described in a simpler manner if one uses the FEL parameter  $\rho_{FEL}$ . Its derivation can be found in [11], here it is given by equation 2.6, where  $n_e$  is the electron density;  $k_u = \frac{2\pi}{\lambda_u}$ ;  $m_e$  is the electron mass. These parameters relate to the plasma frequency oscillations  $\omega_p = \sqrt{\frac{n_e e^2}{m_e \epsilon_0}}$ .

$$\rho_{FEL} = \left( \frac{\mu_0 K^2 e^2 k_u^4 n_e}{4\gamma^3 m_e} \right)^{1/3} \quad (2.6)$$

We can approximate the electric field along the undulator in the low gain regime as  $E = E_0 \exp(z\Gamma\sqrt{3})$  where  $\Gamma = 2k_u\rho_{FEL}$  is the gain parameter. From this, the gain length can be defined as the distance over which the intensity increases by a factor of  $e$ ,  $L_G = \frac{\lambda_u}{4\pi\rho_{FEL}\sqrt{3}}$  [11]. As an example, the FEL whose gain curve is shown in Figure 5 has a gain length of approximately 1.5 m. The plot shown in Figure 5 has two main parts, the first 26 m which correspond to the exponential gain and the final 25 m, where the the FEL reaches saturation. These stages in the FEL process are examined in terms of coherence in the Results section.

The FEL bandwidth is also described in [11] with the help of the FEL parameter  $\rho_{FEL}$  as follows:  $\Delta\omega(z) = 3\sqrt{2}\rho_{FEL}\omega_{lab}\sqrt{\frac{L_G}{z}}$ . Where  $\omega_{lab}$  is the central frequency of the undulator radiation. This equation is valid for the region between  $4L_G$  and the beginning of saturation.

### 2.2.3 SASE and Seeded FEL

In the previous subsection we assumed that the only radiation present was generated from the electrons themselves. In the following, we will consider different FEL based on the mechanism that starts the bunching process and describe each type highlighting their characteristics. In this respect FELs are divided in two main categories, Seeded and SASE.

First we take a look at Self Amplified Spontaneous Emission or SASE FELs. This type of FEL relies on the spontaneous undulator radiation to start the bunching process. This light is, however, not correlated in phase due to random variations in the electron distribution, called **shot noise**. Because of this, the microbunching will be slightly mismatched between different parts of the same electron bunch. The result of this mismatch is a noisy spectrum in which several narrow spikes appear, Figure 6 a).

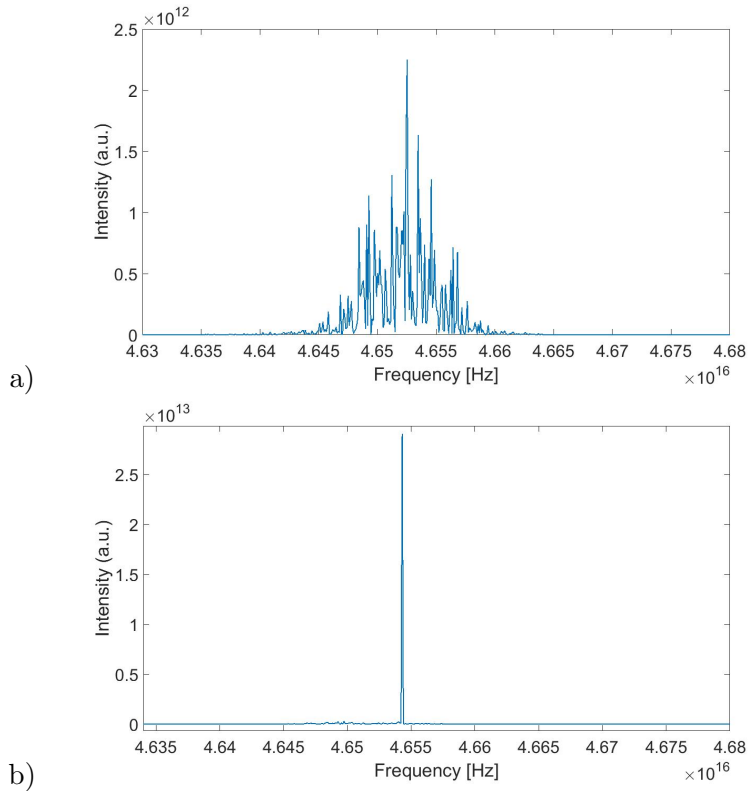


**Figure 6:** Plot representing the spectra of a SASE FEL (top) and a Seeded FEL (bottom) obtained from my own simulations.

For ideal cases, the SASE process was described and analyzed and it was found in [13, 11] that the saturation is reached after  $L_{sat} = \frac{\lambda_u}{\rho_{FEL}} \approx 20L_G$ .

Seeded FELs rely on an externally produced radiation to initiate the microbunching. It is important to note that an FEL becomes seeded if the external radiation has enough power to overcome the randomness that is intrinsic to the electron bunch due to shot noise. If this condition is met, electrons will emit in phase and the spectrum will have a very narrow

bandwidth, Figure 6 b).

There are various schemes for seeding in frequency regions where conventional lasers are unavailable such as the X-ray regime. For these frequencies the seed is actually FEL radiation produced by the electrons at an earlier stage [14]. This arrangement has three main parts: the stage in which SASE radiation is produced, the chicane and monochromator, the final part is a second undulator which acts like a Seeded FEL with the previously produced radiation as seed. A basic layout of the seeding schemes is presented in Figure 7.

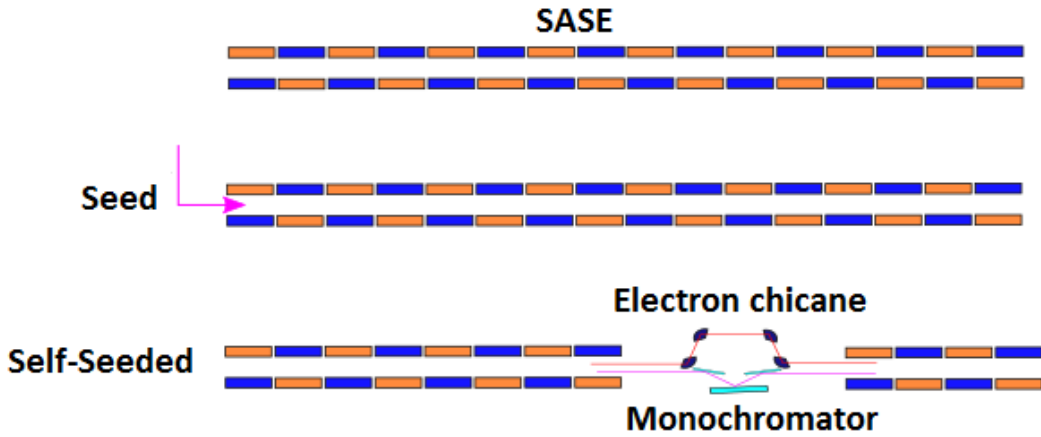


**Figure 7:** Layout of the three types of FEL with their respective components after the electron acceleration. The difference between SASE and Seeded configuration is the presence of the external seed radiation and the undulator can become shorter as in general, Seeded FELs saturate faster. The self-seeded layout is a bit different in that the undulator is split in two. The first part is basically a SASE FEL which does not reach saturation. However the electrons still microbunch and radiation is being produced. Following the first undulator the light enters a monochromator to select one narrow band from the SASE spiky spectrum. The electrons enter into a magnetic chicane which has a two fold action: it delays the electrons so that they correctly overlap with the monochromatized beam; it erases the microbunching from the first undulator. The second part of the undulator behaves like a Seeded FEL where the monochromatized light produced in the first undulator acts as seed.



### 3 Coherence

*This chapter is intended as an introduction to the basic concepts of coherence. Starting from a definition we will explain what coherence is, what purpose it serves and what are the types of coherence that light has. Finally we will try to motivate the use of coherence in describing FEL light.*

Let us consider light produced by a source that has random fluctuations. The monochromatic plane wave description of this light will not suffice, but a statistical approach is better suited to characterize it. The statistical description of the random fluctuations in light is the subject of **coherence**.

For the next two subsections we will use the wavefunction  $U(r, t)$  to describe the light wave. Observing the arguments of the wavefunction, we can divide them into transverse coordinates described by  $r$  and a longitudinal coordinate represented by  $t$ . Following this description we treat transverse and longitudinal effects separately.

As it is a common notation, in the remainder of the section we will use  $\langle A \rangle$  to denote the statistical average of  $A$ , or in mathematical form

$$\langle A \rangle_t = \lim_{T \rightarrow \infty} \frac{1}{T} \int_0^T A(t) dt$$

.

#### 3.1 Longitudinal coherence and Spectral density

The ability of a light wave to interfere with a longitudinally delayed version of itself is given in terms of **longitudinal coherence**. A measure of this is the autocorrelation function  $\Gamma$  which is defined in [15] as:

$$\Gamma(\tau) = \langle U(r, t)U^*(r, t + \tau) \rangle \quad (3.7)$$

If we make  $\tau = 0$  we find a familiar physical quantity called average intensity  $I(r) = \langle U(r, t)U^*(r, t) \rangle$ . To show the importance of statistical averaging let us consider the instantaneous intensity  $I(r, t) = |U(r, t)|^2$  and calculate it with data from FEL simulations. Figure 8 shows that the apparently random distribution of intensities illustrated in b), becomes a well shaped Gaussian distribution when averaged a).

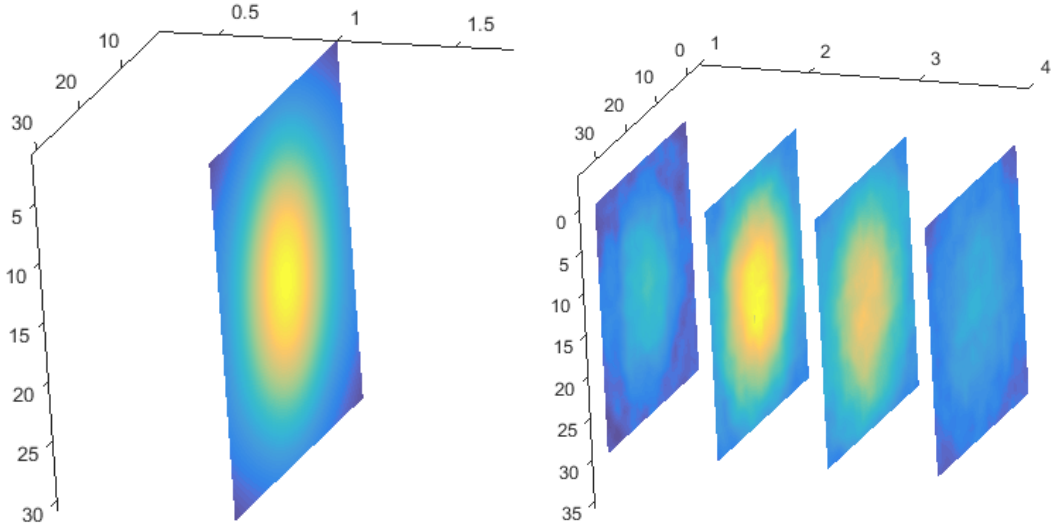


**Figure 8:** Intensity plot of FEL light a) average intensity b) instantaneous intensity at 4 equally spaced positions in the pulse.

There is an intrinsic relation between the autocorrelation function  $\Gamma(\tau)$  and the power spectral density given by :  $S(\nu) = \int_{-\infty}^{\infty} \Gamma(\tau) e^{-2i\pi\nu\tau} d\tau$  , this equation is known as the **Weiner Khinchin Theorem** [16]. If the power spectral density is known, one can also find the autocorrelation function and vice-versa.

It can be convenient to use the normalized version of the autocorrelation function  $\gamma(\tau) = \frac{\Gamma(\tau)}{\Gamma(0)}$  which is called the complex degree of coherence. A more intuitive way of describing longitudinal coherence is through the coherence time  $\tau_c = \int_{-\infty}^{\infty} \gamma(\tau) d\tau$  [15]. In this report the results of longitudinal coherence are presented in terms of coherence time for practical reasons.

Since *Genesis 1.3* generates the field distribution as a function of time, it is easy through Fourier Transform to obtain the spectrum using the Weiner Khinchin theorem. Below we list the relation between  $\Delta\nu$ , which is the FWHM of the spectrum, and  $\tau_c$  for 3 of the most common types of lineshape [15]. For simplicity we use the first relation  $\tau_c = \frac{1}{\Delta\nu}$  without any loss in information. If we assume the same lineshape, the multiplication constants disappear by simple division.

- $\tau_c = 1/\Delta\nu$  Rectangular
- $\tau_c = 0.663/\Delta\nu$  Gaussian
- $\tau_c = 0.332/\Delta\nu$  Lorentzian

### 3.2 Transverse coherence and Young's experiment

In Figure 10 b)  $r_1$  and  $r_2$  are two random points in the (x,y) coordinate system, transverse coherence is a measure of how well these points are correlated. The statistical value that characterizes this property is called the mutual intensity function and its analytical form is given by:  $G(r_1, r_2) = \langle U(r_1, t)U^*(r_2, t) \rangle$ . In measurements however, its normalized form is more useful  $g(r_1, r_2) = \frac{G(r_1, r_2)}{\sqrt{I_1 I_2}}$  and this is the one we use in this report.

Mutual intensity properties are best studied using Young's experimental setup presented in Figure 9. To mathematically describe the intensity at the screen we make some simplifying assumptions: we look at the intensity distribution at the center of the screen to avoid loss of coherence due to time difference; we assume approximately the same intensity at the two pinholes  $I_1 = I_2$ ; the light is quasi monochromatic (this is the case in FELs). Having made these assumptions we can write [16]

$$I = 2I_0[1 + |g(r_1, r_2)| \cos \phi], \quad (3.8)$$

where  $\phi$  is the phase of the complex number  $g(r_1, r_2)$ . The maximum intensity value is found where  $\phi = 0$  and the minimum where  $\phi = \pi$ .

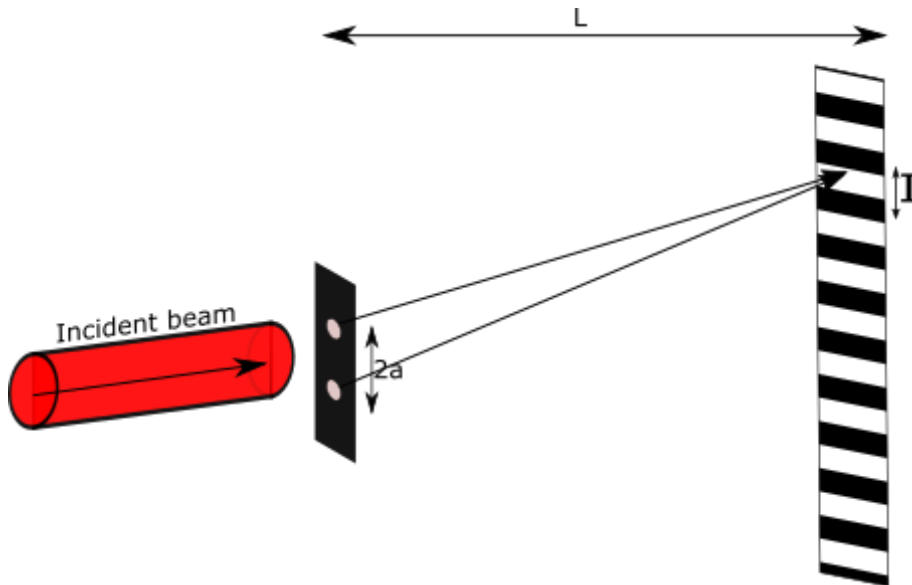


**Figure 9:** Schematic layout of the Young Interferometer in which the distance between the two pinholes is  $2a$ ; the distance between the pinholes and the observation screen is  $L$ ; the distance between two maxima or two minima is noted with  $I$ .

The connection between what we can measure, which is the interferogram at the screen, and the mutual intensity function is made through a parameter called visibility ( $\mathcal{V} = \frac{I_{max} - I_{min}}{I_{max} + I_{min}}$ ). It characterizes how well we distinguish between an adjacent maximum and minimum in intensity. If we introduce this into equation 3.8 we get  $\mathcal{V} = |g(r_1, r_2)|$ , which means that the visibility of the interferogram is a direct measurement of the transverse coherence.

Some considerations about the Young experiment should be made to better understand the nature of the results. Due to the spectral width of the radiation, the fringes on the edges have low visibility. Each pinhole produces its own Airy pattern which limits the distance between the two pinholes. If the distance between two maxima is smaller than the Airy pattern, the visibility is also affected. It is also worthwhile to remember that the young experiment gives the coherence properties at the position of the pinholes and not in the plane of interference. This means that no matter how the interference pattern is obtained it contains the same information about the coherence at the two pinholes.

The mutual intensity is just a special case of a much broader function called mutual coherence which also takes into account the effects of time delay on the mutual intensity.

$$G(r_1, r_2, \tau) = \langle U(r_1, t) \rangle + \langle U(r_2, t + \tau) \rangle \quad (3.9)$$

To better illustrate the types of different coherence parameters let us look at Figure 10. Here a beam of light is represented in the  $(x,y)$  transverse plane and in time.

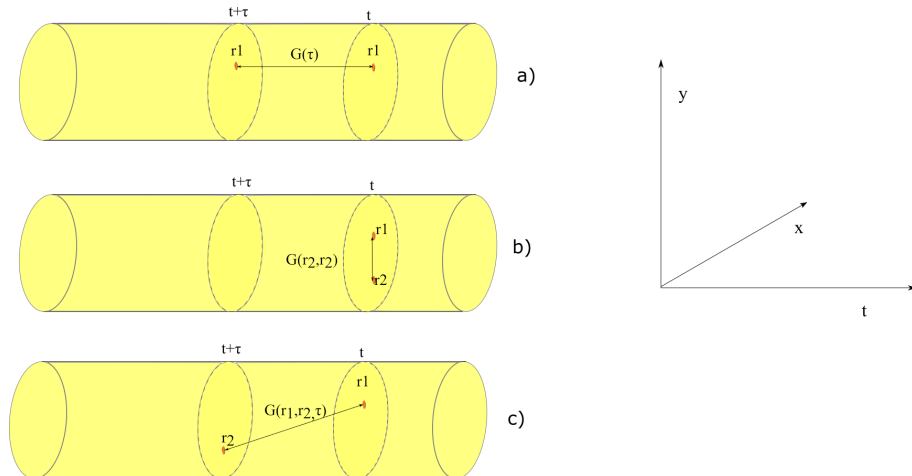


**Figure 10:** Representation the statistical functions describing the Coherence. a) temporal relating the same point in the transverse plane but with a time delay; b) transverse coherence through the mutual intensity function relating different transverse points without any time delay; c) mutual coherence that relates different transverse points with a time delay.

## 4 Simulations

*The simulations chapter will offer information on the basics of Genesis 1.3 software, and present the ways in which relevant information is extracted from its output via additional software such as MATLAB.*

While the first part deals exclusively with the simulation software, the second part of the chapter describes my approach to extracting the desired information from the simulations and to obtaining actual physical values. To best understand the analysis process, some parts will be explicitly described as the code developed as a part of this thesis and may prove useful for further applications.

### 4.1 Overview of *Genesis 1.3*

The *Genesis 1.3* software was initially developed as a part of a Ph.D. at DESY, Germany, by Sven Reiche. It simulates the motion of the particles and the produced radiation in either time-dependent (TD) or time-independent (TI) solutions in a single pass through the undulator. Time independent simulations run in a fraction of the time needed to run time dependent simulations and serve as initial investigation for the input parameters. However, only time-dependent simulations give a physical picture of the phenomena in an FEL

*Genesis 1.3* uses discrete units called "slices" to characterize the e.m. field and particles at specific positions in the undulator. Here lies the distinction between TD and TI simulations. In a TI run just one distinct slice is simulated and that slice is then repeated many times to generate the complete electron bunch and radiation field. This means that the electron distribution and the field appear uniform in time (no time dependency). When running TD simulation many different slices are simulated, each slice having its own electron and field distribution. By analyzing the sequence of slices one can create a picture of the time evolution of the field and particle bunch.

Users are able to simulate a wide variety of FEL schemes by controlling the parameters in the main input file. *Genesis 1.3* makes it possible to import files of particle distribution obtained from software that simulate the production and acceleration of electrons and even radiation files that describe an externally produced e.m. field. The result of such a series of software that follows the electrons from the place where they are produced to the end of the undulator where they are dumped are used to make a "start-to-end" simulation.

In Figure 11, there is an intuitive explanation on how *Genesis 1.3* goes about simulating the FEL process. Along with the illustration, the following input parameters can serve as an initial picture of how the simulation code works. For a more in depth understanding refer to the *Genesis 1.3* manual [17].

- The simulated particles are not electrons but rather macro particles. The total charge remains the same but is divided between the macro particles in order to have reasonably small number of variables during simulations <sup>1</sup>. The number of macro particles ( $N_{part}$ )

---

<sup>1</sup>in a 2 nC bunch, which is less than the bunch used in these simulations, there are more than  $10^{10}$  electrons.

has to be sufficiently large as to not encounter numerical noise. In these simulations the number of particles I used is 8192.

- $N_{car}$  is the number of grid points of the grid in which the e.m. radiation is discretized. In the simulations the magnetic component of the electromagnetic field is ignored
- the wavelength (in meters) is defined by  $XLAMDS$
- the undulator period(in meters) is defined by  $XLAMD$
- the integration step is defined by  $DELZ$  in terms of undulator period length  $XLAMD$
- As discussed above at each integration position, the field is discretized in time "slices". The variable that defines the separation of these slices in terms of number of wavelengths is  $ZSEP$ , and the separation in time of these slices at a given position is defined by  $ZSEP * XLAMDS/c$

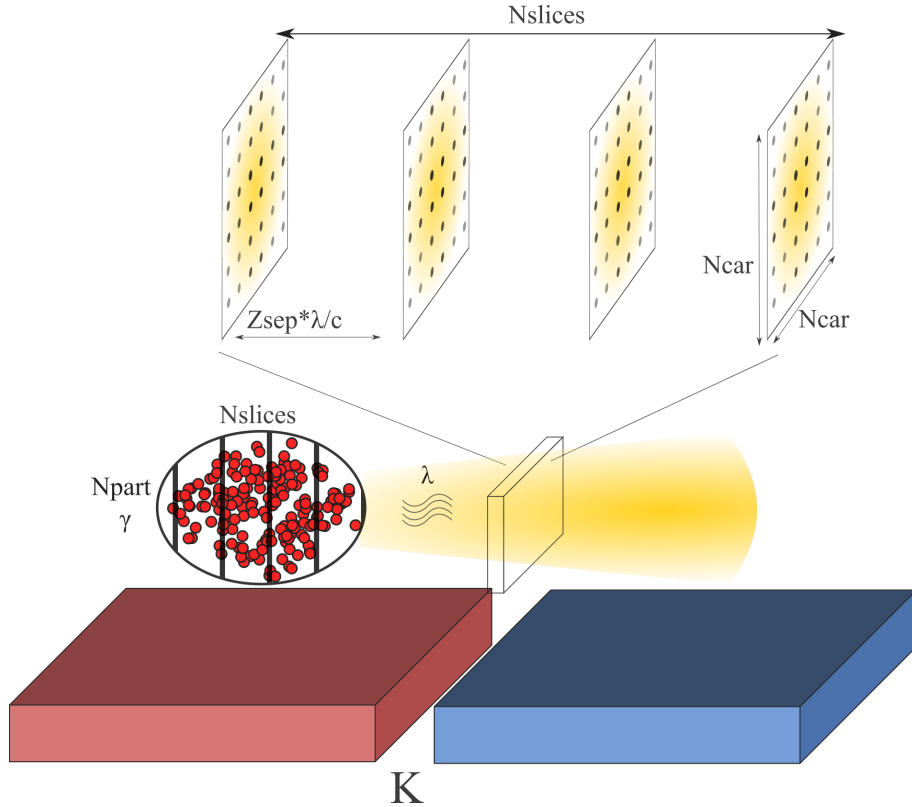


**Figure 11:** Illustration of how *Genesis 1.3* simulates the FEL process.  $N_{part}$  particles spread out in  $N_{slices}$ , simulate the electron bunch. These particles emit radiation at a wavelength  $\lambda$ , given by the electron energy  $\gamma$  and the  $K$  parameter as in equation 2.4. At a given position the field is discretized in the same number,  $N_{slices}$ , time grids. The different grids are equally spaced in time by  $ZSEP * \lambda / c$ . Each grid has  $N_{car}$  by  $N_{car}$  equally spaced points where the e.m. field is saved.

#### 4.1.1 Input and output

*Genesis 1.3* has a large number of input parameters making it suitable for complex simulations where a fine control of the beam, lattice structure, magnetic and trajectory errors is needed. The output is also controlled through flags set in the main input file.

As the focus of this thesis is the coherence of the generated radiation, the field output file will be discussed more in-depth in the following. *Genesis 1.3* records the field at a specific point in time at a specific position in the undulator, as an  $N_{car} \times N_{car}$  matrix of complex number. The ".fld" file is a collection of  $N_{slices}$  matrices at each position in the undulator where the field is saved.

It is important for the following subsections to state that, when read, the information in the field file is discretized in a 4D matrix. The first dimension refers to the position along the undulator. The second dimension represents the time evolution of the field at a specific position. Incrementing this dimension by 1 "jumps" in time by  $XLAMDS * ZSEP$ . The last two dimensions represent the transverse coordinates in the (x,y) plane. The distance between two consecutive points in either direction is calculated by the program based on the electron distribution size, wavelength and the seed laser Rayleigh length and waist.

## 4.2 Analysis

Once the field file is read in the form of a 4D matrix we can start analyzing the data in terms of coherence. For this purpose we work our way through the field and perform calculations at each point in the undulator where the field was saved. In Figure 12, an intuitive display of the matrix is presented. This matrix is used for both longitudinal and transverse coherence measurements.

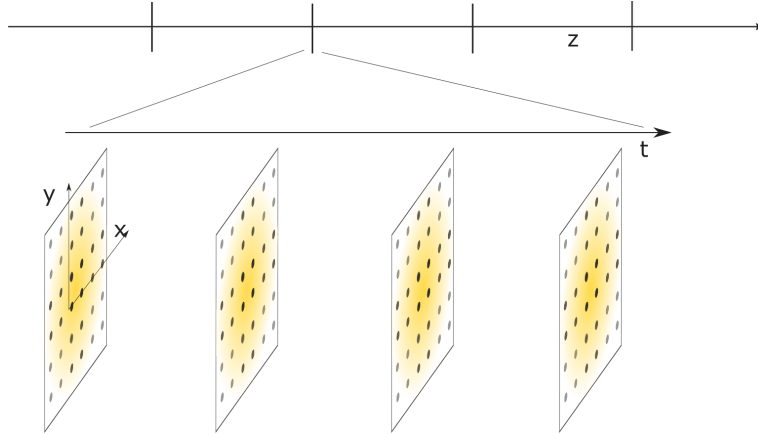


**Figure 12:** Deconstruction of the 4D matrix in which the field information is stored during analysis.  $Z$  describes the position in the undulator;  $(x,y)$  specifies the transverse coordinates;  $t$  represents the time evolution of the field.

### 4.2.1 Spectrum and coherence time

As discussed above, the coherence time and the bandwidth are connected, therefore once the spectrum is obtained one needs only to calculate the bandwidth and from that, the coherence time is uniquely determined.

To generate the spectrum from the matrix representing the field, we need to select the desired position in the undulator and keep the respective index fixed. Then we need to select the point on the transverse grid where we want to study the longitudinal coherence<sup>2</sup>. With the three spatial coordinates fixed, we apply the Fourier transform on the remaining dimension (time) resulting in the electric field vs frequency vector. The intensity vs frequency is obtained by calculating the absolute value of the field  $|E|^2$  and plotting it against the frequency.

In the SASE case, since it is composed of many individual narrow peaks, it is more difficult to extract the bandwidth. The method used in these calculations involves smoothing around the spikes to the point where only a single broad peak is obtained. The FWHM of this peak serves as the bandwidth  $\Delta\nu$  of the spectrum. In the case presented in Figure 13,  $\Delta\nu = 1.816$  THz which when using the relation  $\tau_c = 1/\Delta\nu$  corresponds to a coherence time of  $\tau_c = 5.3fs$ . As a comparison the Seeded spectrum has a bandwidth of  $\Delta\nu = 2.07GHz$  which corresponds

<sup>2</sup>We usually want to select the point which has the most intensity but one can select any other point.



to a coherence time  $\tau_c = 482fs$ .

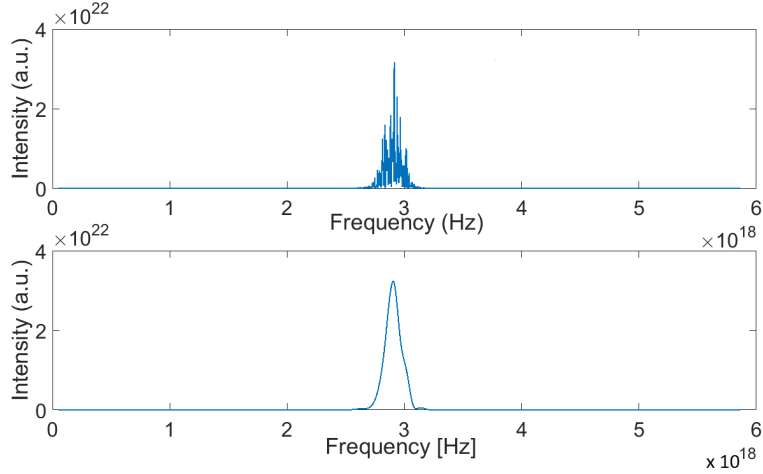


**Figure 13:** Plot representing the unaltered spectrum of SASE FEL (top) and a the smooth spectrum (bottom).

### 4.3 Virtual Young’s experiment

Transverse coherence describes the ability of two points in the transverse plane to interfere with each other. In the coherence section we suggested the Young experiment as a way to extract the mutual intensity information from the field. Now we aim to describe how a Young experiment can be performed, virtually, on an e.m. field discretized in a 4D matrix.

From a grid that represents the average intensity in the (x,y) plane we select the two points that we want to describe in terms of transverse coherence. Afterwards, we construct a mask to block all other points in the grid. For reasons which will become apparent in the following paragraphs, we tilt the mask to have the points on a horizontal line in the center of the mask. Using a 2D Fourier transform<sup>3</sup>, we construct the interference pattern from the two points. This process is repeated for all the time slices and the interferogram is constructed by adding all the interference patterns.

The selection of the mask has an important role in the experiment and thus needs to be chosen very carefully. The construction of the field immediately after the mask involves copying the field at the selected points on a blank 2D matrix keeping the same distance between them. The size of the blank matrix has to be sufficiently large as to not influence the visibility of the interference pattern. After many trials we settled on the following formula to calculate the size of the matrix  $l = 3d$ ,  $L = 30d$  where  $d$  is the distance between the selected points in the original grid. Increasing the matrix size further will only improve the visibility by 0.1%, which we find acceptable. One can select any two points on the grid, but on the blank

<sup>3</sup>One could use a Fourier propagator to simulate the Young experiment with more fidelity but we want to get best possible visibility without having to worry about the distance between the pinholes and the projection screen which may affect the visibility [18]

matrix they will always be copied in the horizontal direction in the middle of the matrix. This process is better illustrated in Figure 14.

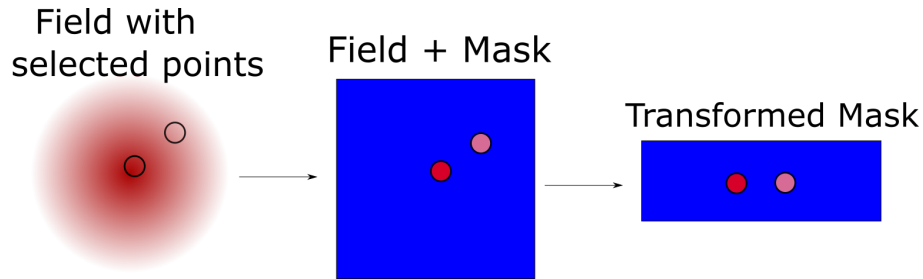


**Figure 14:** Representation of the process of applying a mask to the field for Young experiment.

Having the interference pattern, we extract the visibility and multiply it with the normalized intensity to get the mutual intensity i.e., the measure or transverse coherence. To avoid human error in choosing the point with maximum and minimum intensity *Matlab* has a function (*findPeaks*) that does that for us. The input for the *findPeaks* function is required to be a vector not a 2D matrix (which our interferogram is). Because we placed the points in the middle of the mask we can simply take the middle horizontal line from the interferogram as the vector input for the *Matlab* function.

In Figure 15 a Young interferogram from actual simulations is presented. In Figure a) the two points are well correlated and thus the the visibility has a high value  $\mathcal{V} = 0.92$  while in figure b) the correlation is poor and thus the visibility is only  $\mathcal{V} = 0.55$ .

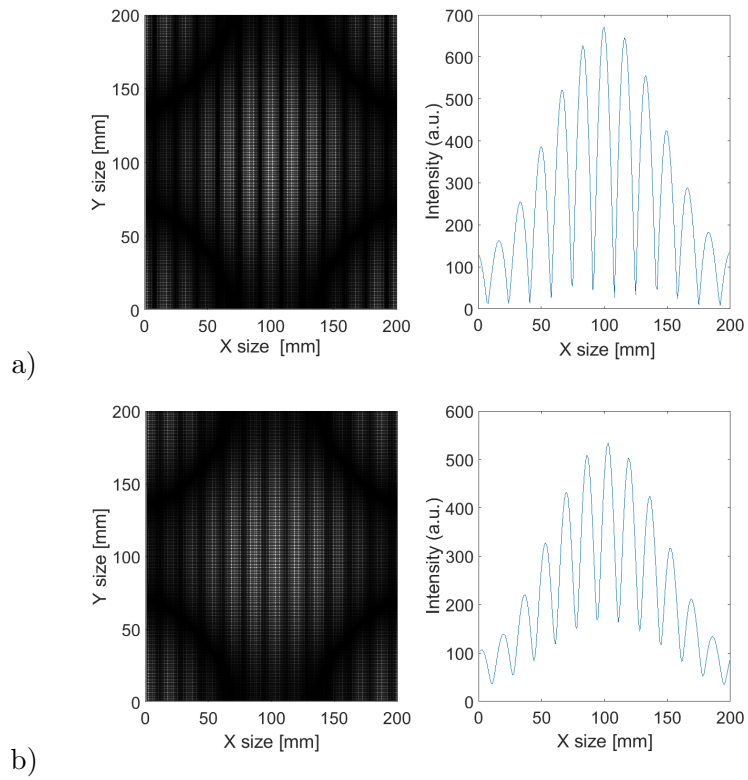


**Figure 15:** Virtual Young experiment output. In a) the field has good transverse coherence between the two points. In b) the field has poor transverse coherence between the two points.

## 5 Results and discussions

In this section we present coherence related results obtained using the methods described in section 4. We look on how coherence is affected by changing different FEL parameters and what new information these results yield.

The simulation input files originate from an adapted version of the input file "ttf-ii.in" from the *Genesis 1.3* website [19]. In table 1, the main parameters of the FEL tested here are listed and are not changed during simulations. Changes were made to the Twiss parameters, seed radiation properties, undulator type as well as to the simulation control parameters [17]. It is important to mention that the simulated "seed" laser is a Gaussian wave and that the waist is located at position 0.

$\lambda$ nm	$\lambda_u$ mm	K	$\gamma_0$	Current A
6.4457	27.3	1.267	1956.947	2500

**Table 1:** Table containing the main FEL parameters.

It is important to control the transverse size of the electron beam. This is done by dividing the undulator into 10 sections and inserting focusing elements between two consecutive sections. The combined length of an undulator segment and the focusing elements is 5 m. For the simulations regarding longitudinal coherence, the field distribution is saved with a period of 3.4 m. For results concerning transverse coherence the field is saved with a period of 5 m<sup>4</sup>, so after each segment with its corresponding focusing structure. The layout of such a structure is depicted in Figure 16.

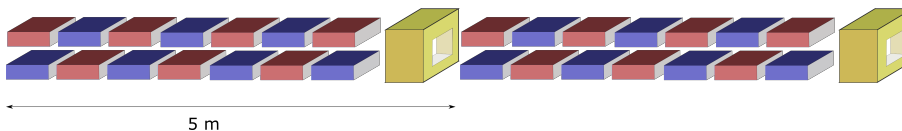


**Figure 16:** Schematic representation of two segments from the FEL with the adjacent focusing element. The alternating red and blue boxes represent the undulator with its periodic magnetic array, and the yellow boxes represent the focusing elements between undulator segments.

When discussing properties of the FEL light along the undulator we want to know where we are in the gain curve (generated power vs position) of the FEL. It is desirable to see if there is any direct connection between the coherence properties and the different stages of the gain curve. To make it easier to see where we are in the gain curve, Figure 17 shows the power with respect to position plot for different seed power .

---

<sup>4</sup>Because the e.m. field gains transverse coherence when propagating through free space, we had to make sure that the field is saved at equivalent positions in the undulator when calculating transverse coherence properties

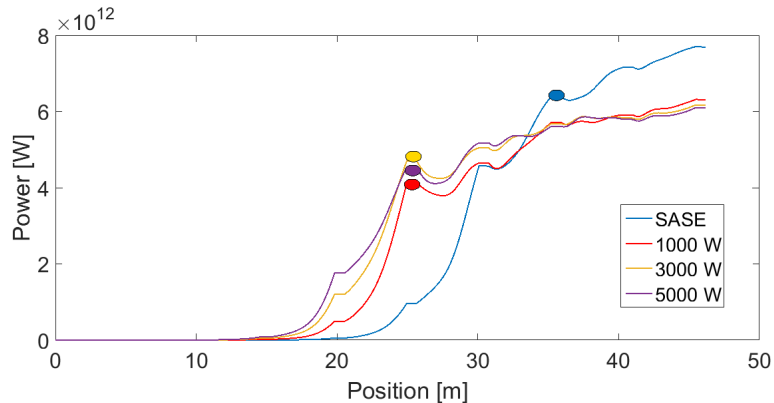


**Figure 17:** Power output at different positions in the undulator for different seed power. The thick colored points represent my assessment of where the saturation begins for each seed power.

The plot in Figure 17 shows that by seeding, saturation is achieved at an earlier stage in the undulator and we expect some coherence properties to change accordingly. We infer from the plot that when seeded, the FEL saturates at 25 m and when in SASE mode the studied FEL saturates at 35 m. Furthermore we can see no influence on the position of the saturation point by increasing the seed power. The straight horizontal lines in the power plot represent the power at the position of the focusing elements. Because there is no undulator at these positions, electrons do not produce any power output.

## 5.1 Longitudinal coherence results

The coherence time for the SASE run is calculated as described in the previous section. The evolution of the coherence time at different points in the undulator is shown in Figure 18. It can be seen that the plot has a maximum of  $\tau_{SASE} = 11 \text{ fs}$  at 25 m. The maximum in coherence time is achieved 10 m before power saturation. This means that the longitudinal coherence *saturates* faster than the gain curve in Figure 17.

It is obvious from the Figure 18 that the coherence time drops as the process approaches saturation. This can be explained by the fact that very close to saturation the microbunching of the electrons is worse, hence the emitted radiation has larger bandwidth and worse coherence time. The fact that the coherence time reaches its maximum before saturation, could be used to predict where the FEL process will saturate.

Based on the number of time slices ( $N_{slices} = 2400$ ) and on the time interval between them  $\Delta t = 0.21 \text{ fs}$  we have a total simulated time window of  $T = 500 \text{ fs}$ . When performing calculations on the seeded cases we find that the coherence time  $\tau_{SEED} = 500 \text{ fs}$  is the same as our simulated time window. Furthermore we see no change in the seeded FEL coherence time as we move through the undulator, this means that the simulation time window is not large enough to get the measure of the coherence time for the seeded FEL. Since we could only observe differences in the SASE coherence time along the undulator, we restrict our analysis of the longitudinal coherence for the remainder of this subsection exclusively to studying effects on the longitudinal coherence in SASE mode.

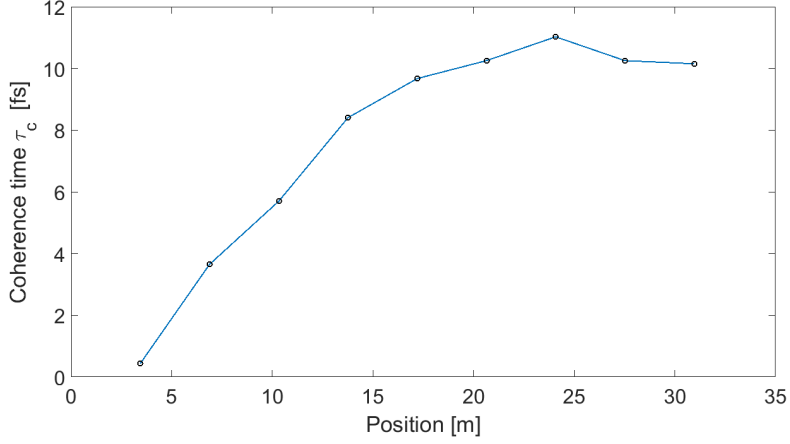


**Figure 18:** Coherence time  $\tau_c$  at different positions in the undulator.

It can be of interest to test if the coherence time is the same for different points in the transverse plane. Figure 19 synthesizes the results of how longitudinal coherence evolves going from the center of the grid, outwards. For that we selected 3 points, each increasingly further away from the center and performed the longitudinal coherence calculations. We observe only small differences between the coherence time of points located in the same plane, for the highlighted part however, the plots representing horizontal and vertical points are mismatched. We can think of these small ripples in the coherence time as periodic perturbations. Looking closer we see that, as the perturbation in  $y$  has a maximum, the perturbation in  $x$  has a minimum and vice-versa which suggests that the perturbations are coupled.

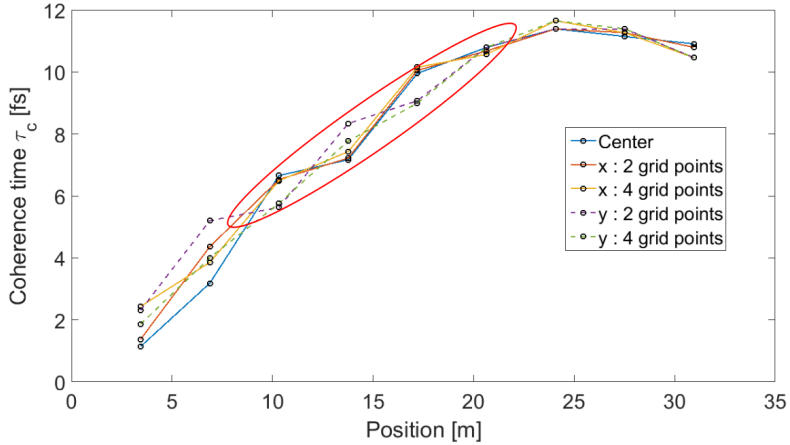


**Figure 19:** Coherence time  $\tau_c$  at different positions in the undulator for 3 different grid points in a planar undulator. The dotted lines show the evolution of the coherence time as we go outwards from the center in the vertical direction and the continuous line shows what happens to the coherence time as we move in the horizontal plane. The discrepancies between the horizontal and vertical direction are highlighted in the red ellipse.

In trying to learn more about these perturbations I proposed switching from a planar undulator to a circular one. In the planar undulator the electrons only oscillate transversely in the x plane, so the field may have different properties in the x direction due to this fact. In a circular undulator, the electrons describe a circle in the transverse plane (the final 2 dimensions of the 4D matrix). This means that their trajectories are now similar in the x and y plane, which could make the coherence times more similar as well.

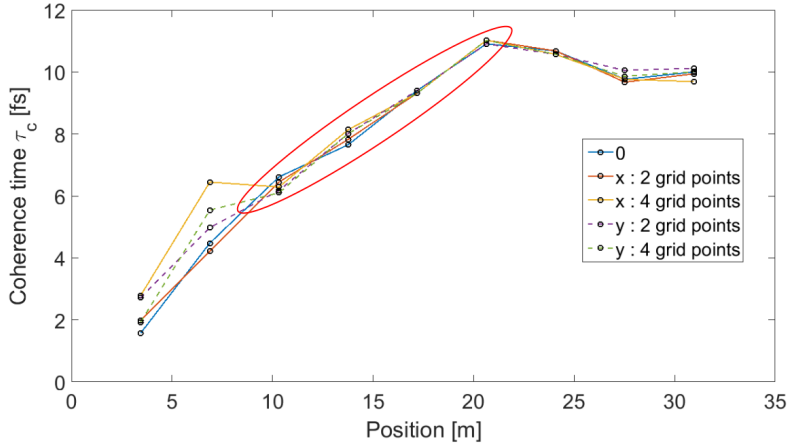


**Figure 20:** Coherence time  $\tau_c$  at different positions in the undulator for 3 different grid points in a circular undulator. The dotted lines show the evolution of the coherence time as we go outwards from the center in the vertical direction and the continuous lines show what happens to the coherence time as we move in the horizontal plane. The continuous blue line represents the evolution of the coherence time in the center of the grid. The same area as in Figure 19 is highlighted in the red ellipse.

Moving to the circular undulator (Figure 20), we see that indeed the shape of the plots is much smoother for the highlighted part, meaning that changing from planar to circular undulator type, has eliminated the perturbation. The reason for this improvement can be a subject to future research, for now we can only speculate about it. However, there are a few unexpected changes as well. Firstly the coherence time at 4 grid points away from the center in the horizontal plane has a local maximum at 6 m which was not present in the planar case. Since this phenomenon is happening in the early stages of amplification and in the outer areas of the grid where the radiation is weaker, we assume it is due to numerical noise.

The second difference is the fact that in the circular undulator the coherence time has the maximum value at an earlier position than in the planar case but the actual coherence time is lower than in the planar undulator. Explaining this behavior requires further work but, the initial assumption is that the coherence time saturates earlier than in the planar case.

## 5.2 Transverse coherence results

We start our analysis from SASE simulations and look on how the transverse coherence evolves along the undulator. We go on to compare how the seed power affects transverse coherence. Finally we fix the seed power and analyze the effect of the Rayleigh length of the seed. Since we perform qualitative analysis we can use the visibility which is the normed absolute value for the mutual intensity function.

The transverse correlation of the field is characterized with the Young double pin hole experiment which was described in section 4.3. We use two methods when selecting the two points for the Young experiment. The selection is either symmetric or fixed point, these two methods yield complementary information about the coherence properties of the field. The way in which each selection of points happens is presented in Figure 21.

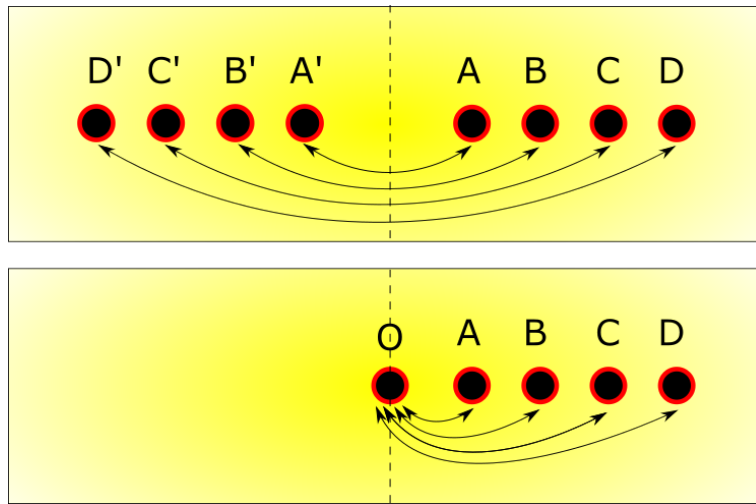


**Figure 21:** Schematic representation of the two selection modes Symmetric (top) and Fixed point (bottom). In the Symmetric mode the two points selected for the Young experiment are located symmetrically with respect to the center of the matrix, A is selected with A', B with B' and so on. The points A, B, C, D are increasingly further away from the center. In the Fixed point mode the center point is kept fixed in the center of the grid and forms pairs with each of the remaining points A, B, C and D.

We first look at the results for points located symmetrically from the center. This is representative of how "LASER-like"<sup>5</sup> the FEL radiation is. In Figure 22 a) the results of calculations from data saved at the end of each undulator section are presented. When looking at it, this graph has two features that stand out. The first one is that for the first point in the graph, corresponding to 0 meters into the undulator, the visibility has a value of 1 which represents a perfect laser beam. Even though SASE should have no Seed, the residual numeric values<sup>6</sup> are evident here because the electrons have yet to produce any radiation at

<sup>5</sup>How well the Gaussian shape is held or how symmetric it is

<sup>6</sup>*Genesis 1.3* does not handle in the input a value of "0 W" for the seed radiation, that is why usually the input is very low  $10^{-15}W$  but not 0. So a seed laser is simulated but with very low power so it can not overcome the shotnoise power of the electron bunch



0 meters. The second feature is the overall similar shape of the plots and the fact that they all converge to the same value (within 0.5%).

Using the fixed point selection method, we find the results that are depicted in Figure 22 b). It is obvious from the definition of the visibility in section 3 that the a maximum theoretical value is 1. This value can not be reached since the wavefront would have to be perfectly flat and have the same intensity at all the selected points. The fixed point measurements are rather an indication of how flat the wavefront and the intensity distributions are. With the exception of the first point, which is only representative for the seed laser, the evolution of the visibility plots are similar for all studied distances between points.

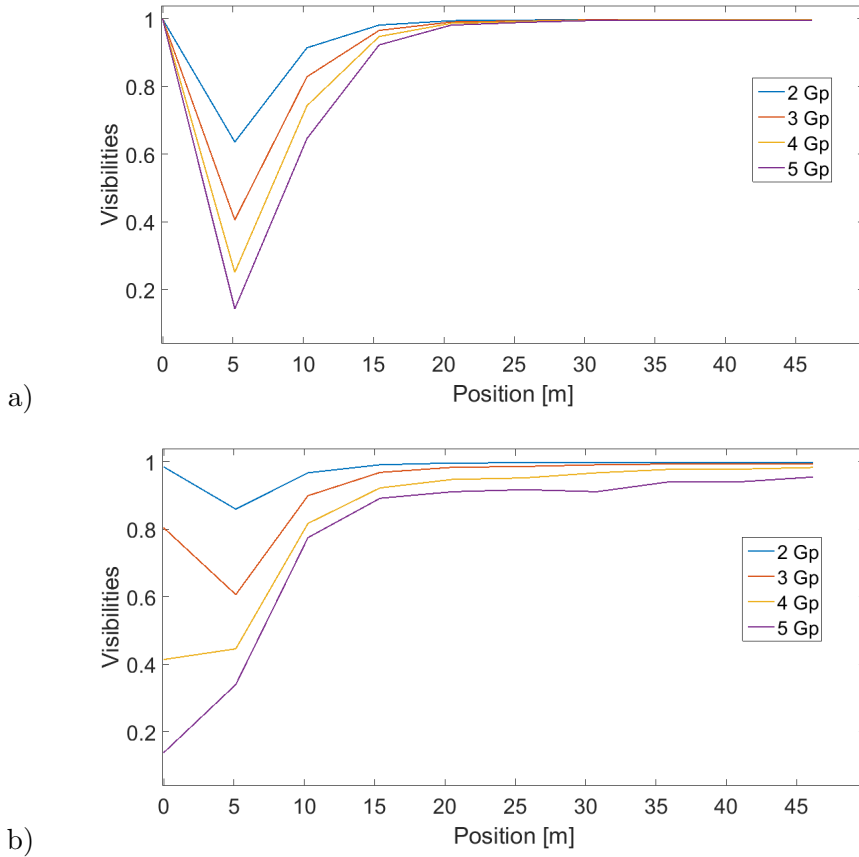


**Figure 22:** Visibilities from the Young experiment with points located a) symmetrically with respect to the center, b) with the center point fixed, for SASE simulations. We restricted our analysis to 5 grid points since the intensity drops to half at 5 grid points away from the center.

The results presented in Figure 22 b) suggest a somewhat contradictory picture. If we look at the Visibilities at 0, which correspond to the seed laser, we see they are lower than the values reached at 35 m for example. This is counterintuitive if we just think that the seed laser is ideal. However when we take into account the fact that the measured waist for the seed laser is 3 grid points or 25  $\mu\text{m}$  we see that the ideal seed laser varies greatly in

intensity between 2 and 5 grid points so the corresponding fixed point analysis basically shows that the output FEL radiation is more uniformly distributed over the 5 grid points considered.

We can use the fact that we are running simulations as the basis for our results and decouple the effect of the intensity and the angle on the total visibility. To evaluate which of these two has more influence on the transverse coherence we have performed the young experiment calculations on the complex field, on the absolute value of the field and on just the angle between the complex and real part of the field. The results of these calculations are presented in Figure 23 . For this illustration we used a seeded FEL (1000 W) as to rule out the possibility of numerical noise at 0 m, where the only radiation is the Seed in both fixed point and symmetric selection mode.

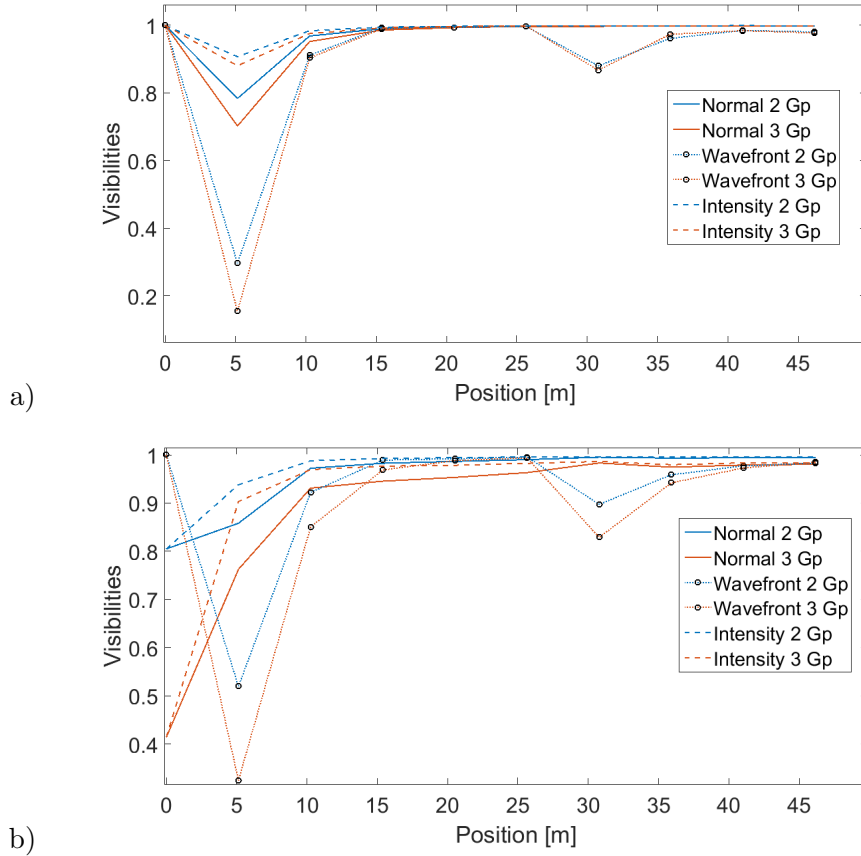


**Figure 23:** The decoupling of the angle and the intensity with respect to the total field in the Young experiment for two different point selections. The continuous line represents the normal Visibilities, the dashed line represents the results for the intensity and the dashed with a marker represents the results for calculation performed on the angle of the field. The two plots represent a) symmetric b) fixed center point selection mode.

Analyzing the two plots in Figure 23 we can see that the predominant influence on the visibility of the complex field is the intensity distribution. With the exception of the second point (at 5 m) where the intensity is distributed almost randomly in the transverse plane and

the phase has a stronger effect, the *normal* line follows the *intensity* line. So if the intensity is more uniformly distributed at a latter point in the undulator, the visibility of the produced radiation is better than the seed laser visibility in fixed point calculations.

The power of the seed laser may also have an impact on the coherence in the transverse plane. In order to show this effect we ran simulations for 4 different seed power, starting from SASE all the way to 5000 W (the calculated shot noise power is 580 W for this example). Due to the fact that for all studied distances, the evolution of the visibilities plots is similar for all distances between points, we can select just one distance as representative for the general behavior. In this case, 3 grid points was the selected distance.

After calculations, we summarized the results in Figure 24. A qualitative analysis tells us that the transverse coherence for a fixed distance between the studied points is not dependent on the seed power at saturation even though it varies significantly in the high gain region. This result holds for both symmetric and fixed point calculations. The same conclusion regarding the fixed point analysis can be drawn here, the visibility after 15 m exceeds the visibility of the seed laser which means that the FEL generated field is more uniform, for the selected points, than the seed.

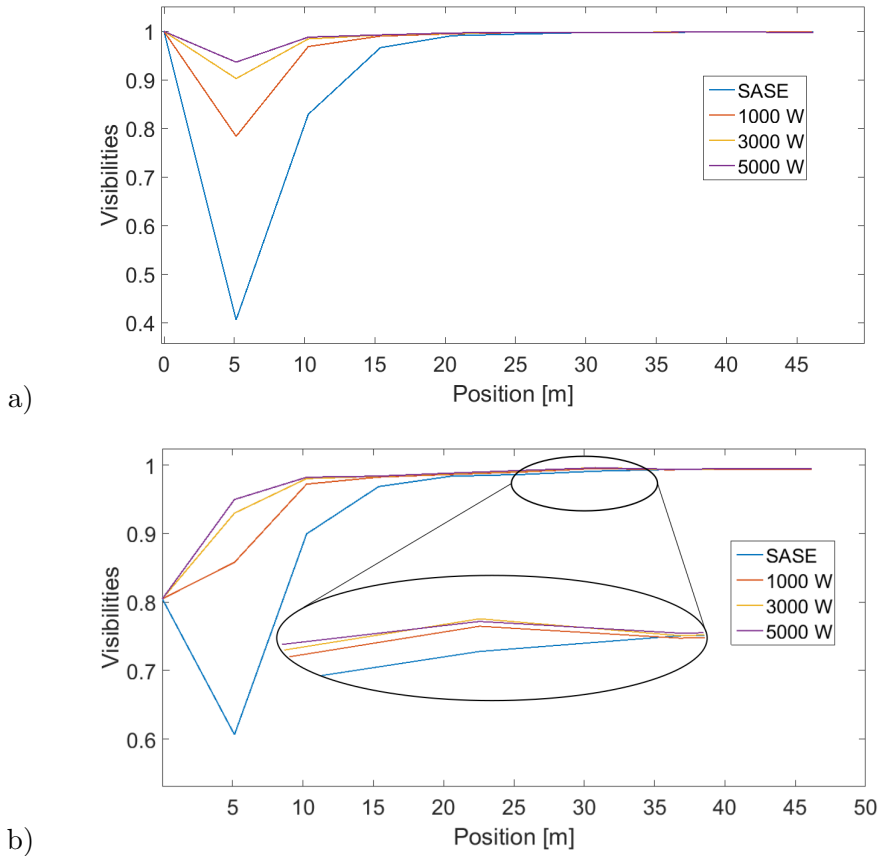


**Figure 24:** Visibilities from Young experiment with different seed power. a) symmetric b) fixed center point.

When looking closely at Figure 24 b) at 30 m, one can see that the results for seeded simulations have a local maximum in that region. If we compare the position of the power saturation (Figure 17) to this position, we can see that the transverse coherence maxima are one undulator section after the position where the FEL reaches saturation in the seeded cases. The interpretation in this case is that as the FEL reaches saturation the electrons tumble in phase space to negative phase (the electrons take power from the radiation) and no new radiation is produced. The previously produced radiation propagates, and in doing so gains transverse coherence [15], reaching the maximum we see. After some distance the electrons have positive phase again and new radiation, which overpowers the more transversely coherent radiation, is produced.

Considering the previously presented result, that the FEL output radiation has a more uniform distribution of intensity than the seed laser, we now examine how does the size of the seed laser affect transverse coherence. To study this phenomenon we ran simulations in which the Rayleigh length of the initial seed laser is changed. In Figure 25 we show the evolution of the visibility through the undulator for different Rayleigh lengths.

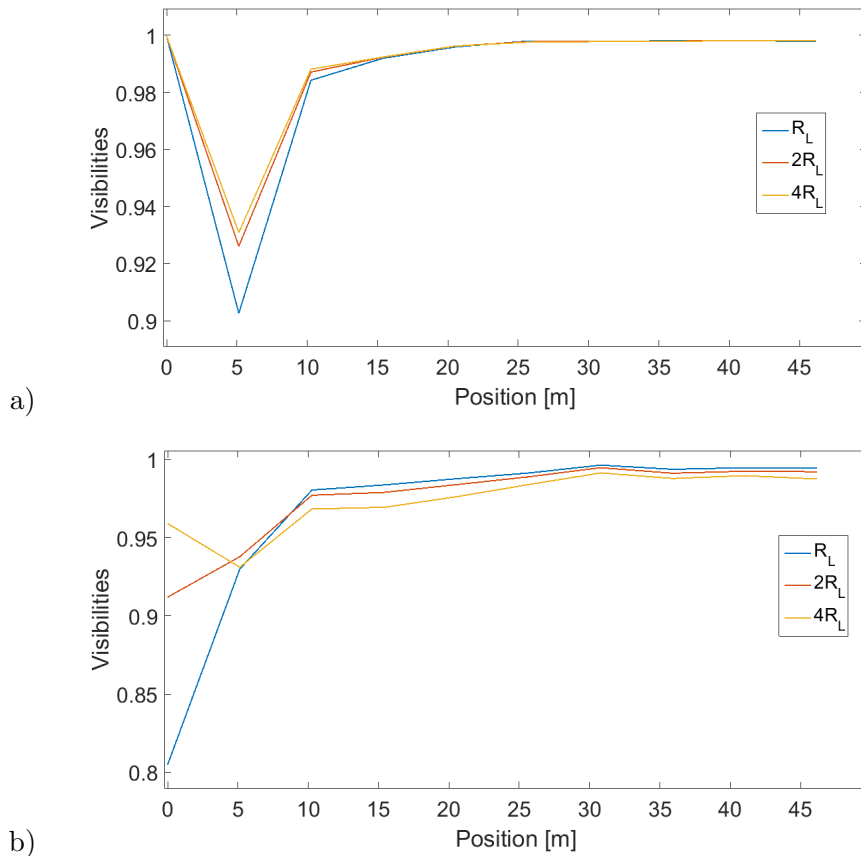


**Figure 25:** Visibilities from Young experiment with different Rayleigh lengths of the seed. a) symmetric b) fixed center point.

In order to have a larger size of the seed Laser we effectively distribute power from the

center of the laser beam to the sides thus losing power density. Here rises an important question about what do we gain in the trade-off between power density and more uniform intensity distribution in the seed laser. In these plots, the Rayleigh length is increased by a factor of 2 after each run. Figure 25 a) shows that *Genesis 1.3* increases the waist with increasing the Rayleigh length. The actual relation is  $W = \sqrt{\frac{R_L \lambda}{\pi}}$  [17].

From the plots in Figure 25 one can observe that even though the visibility in the fixed point experiment, for the smallest  $R_L$ , starts of worse it actually reaches higher values than the other ones. This leads us to believe that the uniformity of the intensity distribution in an FEL is dependent on the power density which initiates the FEL process, not on the homogeneity of the Seed laser. This is contrary to our initial perception that a more flat seed i.e. larger waist would produce a more uniform FEL radiation.

The symmetric points analysis shows that in the initial stages of amplification, the transverse coherence is better for larger Rayleigh lengths. However, in saturation, there is no evidence of any influence by the Rayleigh length on the transverse coherence.

## 6 Conclusions and outlook

Using simulation software and purposely designed code I produced a method for analyzing the coherence properties of FEL light. The basic idea for the code is based on two simple experiments that are used in real life to extract longitudinal and transverse properties of the radiation field inside the undulator.

Based on the results from these virtual experiments we concluded that longitudinal coherence reaches its maximum value before saturation and that it is influenced by the type of undulator polarization the FEL has.

Studies performed with the virtual Young experiment suggest that the intensity distribution is the dominant factor for the transverse coherence in an FEL.

The transverse coherence fixed point results showed that the FEL light has a more even distribution of intensity than the seed, for the studied seed Rayleigh lengths. Furthermore, the same results revealed a local maxima located one undulator period after saturation was reached. With further studies this result may prove useful in determining the actual position where saturation is reached in an FEL.

To give quantitative results the analysis tools developed here must be calibrated and tested against real experiments. This would be possible since both of the virtual experiments presented here, reading the spectrum for the temporal coherence and the Young experiment for transverse coherence, have been used to describe the output radiation of FELs.

The project as a whole has produced a tool for studying coherence in FELs. Results presented in this report suggest a strong relation between the coherence properties and the seed and the undulator type. Through the points raised in the results chapter several research directions may be pursued, such as the dependency of the coherence properties on the undulator type and the optimization of transverse coherence with respect to the seed Rayleigh length.

## References

- [1] Oleg Chubar, Marie-Emmanuelle Couprie, Marie Labat, Guillaume Lambert, François Polack, and Olivier Tcherbakoff. Time-dependent fel wavefront propagation calculations: Fourier optics approach. *Nuclear Instruments and Methods in Physics Research Section A: Accelerators, Spectrometers, Detectors and Associated Equipment*, 593(1):30–34, 2008.
- [2] M. Dohlus, K. Flöttmann, O.S. Kozlov, T. Limberg, Ph. Piot, E. L. Saldin, E. A. Schneidmiller, and M. V. Yurkov. Start-to-end simulations of sase fel at the tesla test facility, phase 1. *Nuclear Instruments and Methods in Physics Research Section A: Accelerators, Spectrometers, Detectors and Associated Equipment*, 530(3):217–233, 2004.
- [3] E. L. Saldin, E. A. Schneidmiller, and M. V. Yurkov. Self-amplified spontaneous emission fel with energy-chirped electron beam and its application for generation of attosecond x-ray pulses. *Phys. Rev. ST Accel. Beams*, 9:050702, May 2006.
- [4] A. Singer, F. Sorgenfrei, A. P. Mancuso, N. Gerasimova, O. M. Yefanov, J. Gulden, T. Gorniak, T. Senkbeil, Y. Sakdinawat, A. and Liu, et al. Spatial and temporal coherence properties of single free-electron laser pulses. *Optics express*, 20(16):17480–17495, 2012.
- [5] Ivan A. Vartanyants and Andrej Singer. Coherence properties of third-generation synchrotron sources and free-electron lasers. 2015.
- [6] Ichiro Inoue, Kensuke Tono, Yasumasa Joti, Takashi Kameshima, Kanade Ogawa, Yuya Shinohara, Yoshiyuki Amemiya, and Makina Yabashi. Characterizing transverse coherence of an ultra-intense focused x-ray free-electron laser by an extended young’s experiment. *IUCrJ*, 2(6), 2015.
- [7] V.N. Litvinenko, S. H. Park, I. V. Pinayev, Y. Wu, A. Lumpkin, and B. Yang. Fourier limited micro-pulses in the ok-4/duke storage ring {FEL}. *Nuclear Instruments and Methods in Physics Research Section A: Accelerators, Spectrometers, Detectors and Associated Equipment*, 475(1–3):234 – 239, 2001. FEL2000: Proc. 22nd Int. Free Electron Laser Conference and 7th F {EL} Users Workshop.
- [8] Lutful Ahad, Ismo Vartiainen, Tero Setälä, Ari T. Friberg, Christian David, Mikako Makita, and Jari Turunen. On spectral and temporal coherence of x-ray free-electron laser beams. *Optics Express*, 24(12):13081–13090, 2016.
- [9] S. Roling, H. Zacharias, L. Samoylova, H. Sinn, Th. Tschentscher, O. Chubar, A. Buzmakov, E. Schneidmiller, M. V. Yurkov, F. Siewert, S. Braun, and P. Gawlitza. Time-dependent wave front propagation simulation of a hard x-ray split-and-delay unit: Towards a measurement of the temporal coherence properties of x-ray free electron lasers. *Phys. Rev. ST Accel. Beams*, 17:110705, Nov 2014.
- [10] E.L. Saldin, E.A. Schneidmiller, and M.V. Yurkov. Coherence properties of the radiation from x-ray free electron laser. *Optics Communications*, 281(5):1179 – 1188, 2008.
- [11] Peter Schmüser, Martin Dohlus, and Jörg Rossbach. *Ultraviolet and Soft X-Ray Free-Electron Lasers: Introduction to Physical Principles, Experimental Results, Technological Challenges*, volume 229. Springer Science & Business Media, 2008.

- [12] Klaus Wille. *The physics of particle accelerators: an introduction*. Oxford University Press, 2000.
- [13] C. Pellegrini, A. Marinelli, and S. Reiche. The physics of x-ray free-electron lasers. *Rev. Mod. Phys.*, 88:015006, Mar 2016.
- [14] Johannes Bahrtdt, B. Faatz, R. Treusch, V. Miltchev, and R. Reiniger. The properties of the fel output for self seeding. *Proceedings FEL 2006, on JACOW*, pages 150–153, 2006.
- [15] Joseph W. Goodman. *Statistical Optics*. Wiley, 2000.
- [16] B.E.A. Saleh and M.C. Teich. *Fundamentals of Photonics*. Wiley Series in Pure and Applied Optics. Wiley, 2013.
- [17] *Genesis 1.3 User Manual*.
- [18] David George Voelz. *Computational Fourier optics. [Elektronisk resurs] : a MATLAB tutorial*. SPIE tutorial texts: 89. Bellingham, Wash. (1000 20th St. Bellingham WA 98225-6705 USA) : SPIE, c2011., 2011.
- [19] Sven Reiche. *Genesis 1.3* website, <http://genesis.web.psi.ch/inputfiles.html>, June 2016.



## 7 Appendices

### Appendix A : matlab code for generating Coherence Time

```
%% Generating Frequency vector
function ct=Coherence.time(field,lambda,zsep)
% field The 4D matrix containing the field
% lambda The wavelength read from the .out file
% slice separation read from the .out file
A=size(field);%get the size of the 4D matrix (field)
nslices=A(1);%get the number of time slices slices
c=3e8;
f0=c./lambda;%central frequency for the wavelength inputed in the in file (XLAMDS)
df=f0./2./zsep;
spacing = df/(nslices);
%the smallest frequency difference resolvable
freq=(-round(nslices/2)+1:1:floor(nslices/2));
freq=freq.*spacing +f0;
%generating the frequency vector

%%
choice = menu('Choose a direction','X','Y')
%chose direction in which you want to calculate the coherence
for j=1:A(2)%follow all the positions in the undulator
    k=1;
    while k<=5 %the maximum displacement from the center is 5*2 gridpoints
        if choice==1
            pts=[floor(A(3)/2)+2*k-1,floor(A(4)/2)+1];
        else
            pts=[floor(A(3)/2)+1,floor(A(4)/2)+2*k-1];
        end
        %progress in either x or y dierction

field2=squeeze(field(:,j,pts(1),pts(2)));

Tfield=ifftshift(fft(fftshift(field2)));
%generate the spectrum

[up,lo] = envelope(abs(Tfield),18,'peak');
%applies envelope

A1=find(max(up)/2<up);
%finds at what positions the intensity is higher than half the maximum
b=(max(A1)-min(A1))*spacing;
%the distance between the highest and lowest frequency that obeys the above
%rule

if choice==1

    ct(j,k)= 1./b;
else

    ct(j,k)= 1./b;
end
%saves the values in variable depending on what direction was chosen
```

```
%calculates bandwidth
```

```
k=k+1;
```

```
%increment position
```

```
end
```

```
end
```

## Appendix B : Matlab code for transverse coherence calculations

```
%% Transverse coherence calculator
```

```
% function t=transverse(field)
```

```
V=1;%initialization of the Visibility variable
```

```
Sizeoffield=size(field);
```

```
for j=1:Sizeoffield(2)%calculating visibilities at every position in undulator
```

```
spacing=2;%initialize the spacing between the two points
```

```
while spacing<=6 %the maximum distance from center is 6 grid points
```

```
pts=[floor(Sizeoffield(3)/2)+1-spacing,floor(Sizeoffield(4)/2)+1;floor(Sizeoffield(3)/2)+1,floor(Sizeoffield(4)/2)+1];
```

```
%rendering the points starting from the middle
```

```
width=1;
```

```
%width of the points
```

```
dist=round(pdist(pts','Minkowski'));
```

```
%calculating the distance between the points in terms of gridpoints
```

```
M=20*2*floor(dist/2)+1;
```

```
N=2*2*floor(dist/2)+1;
```

```
%defining the dimensions for the mask
```

```
A=zeros(M,N);
```

```
%defining the mask
```

```
U=zeros(N,M);
```

```
%defining the image plane
```

```
for i=1:Sizeoffield(1) %going through all time slices
```

```
B=squeeze(field(i,j,:,:));
```

```
%acquiring the 2D matrix that defines the field time slice in the x y plane
```

```
A(floor(M/2)-dist-width:floor(M/2)-dist+width,floor(N/2)-width:floor(N/2)+width)=cerc(width).*...  
mean(mean(B(pts(1,1)-width:pts(1,1)+width,pts(1,2)-width:pts(1,2)+width)));
```

```
A(floor(M/2)+dist-width:floor(M/2)+dist+width,floor(N/2)-width:floor(N/2)+width)=cerc(width).*...  
mean(mean(B(pts(2,1)-width:pts(2,1)+width,pts(2,2)-width:pts(2,2)+width)));
```

```
%applying the mask
```

```
U=U+abs(propagate(A')).^2;
```

```
%obtaining the interferogram for the i-th time slice
```

```
end
```

```

H_line=U(floor(N/2)+1,:);
%extracting the middle vector of the interferogram

[Maxima,MaxIdx] = findpeaks(H_line);
DataInv = - H_line;
[Minima,MinIdx] = findpeaks(DataInv);
[Ma,ind]=max(Maxima);
V=(Ma+Minima(ind))/(Ma-Minima(ind))
%calculating the visibility

Vis(j,spacing)=V;
%saving the visibility
spacing=spacing+1;
end

end

```

## Appendix C : Matlab code for propagator

```

function[u2]=propagate(u1)
%Generates the 2D Fourier Transform of u1
%can be changed to Fraunhofer or Fresnell propagator
u1=fftshift(u1);

u2=(fft2(u1));

u2=ifftshift(u2);

end

```